Journal of Engineering Science and Technology Review 18 (2) (2025) 163- 171

Research Article

JOURNAL OF
Engineering Science and Technology Review

www.jestr.org

Surface Defect Detection in High-speed Railway Overhead Contact System Insulators: An Intelligent Approach Using YOLO-v11

Xin Zheng[1], Yuqi Yan [1], Ning Li[2], Xiangquan Li[3] and Wei Huang[3, *]

[1] *School of Artificial Intelligence and Bigdata, Sichuan University of Arts and Science, DaZhou 635000, China*
[2] *School of Automation and Electrical Engineering, University of Science and Technology Beijing, Beijing 100013, China*
[3] *School of Information Engineering, Jingdezhen University, Jingdezhen 334000, China*

Received 9 December 2024; Accepted 20 March 2025

Abstract

Insulators are indispensable components of high-speed railway overhead contact systems (OCS), continuously subjected to environmental stressors such as lightning, heavy rainfall, strong winds, and ice or snow accumulation. Extreme climatic conditions, including high and low temperatures, also pose further risks of degradation. At present, insulator defect detection predominantly relies on manual data collection and analysis, which is inherently limited in efficiency and accuracy, increasing the likelihood of missed detections and false positives. To address the challenge of intelligent defect detection for OCS insulators, this study proposed a novel detection framework that integrates insulator positioning and precise defect identification, leveraging the YOLO-v11 network. Initially, an insulator device positioning model (IDPM) was employed to locate insulators within OCS inspection images. Subsequently, an insulator defect detection model (IDDM) was utilized to identify insulator defects with high precision. Furthermore, a comprehensive OCS inspection image dataset, encompassing 20,000 images of silicone rubber insulators and ceramic insulators, was constructed. Experimental evaluations on this dataset demonstrate that the IDPM achieves an accuracy of 0.976 and a recall rate of 0.987 in insulator localization. On this basis, the IDDM attains an accuracy of 0.954 and a recall rate of 0.910 in insulator defect detection. Comparative analysis indicates that the proposed method surpasses five state-of-the-art insulator defect detection approaches, highlighting its significant potential for application in OCS maintenance and defect analysis. This research facilitates intelligent status monitoring of OCS insulators, mitigating reliance on manual inspection and contributing to the advancement of automated and intelligent maintenance strategies for high-speed railway systems.

Keywords: OCS, Silicone rubber insulator, Ceramic insulator, Surface defect detection, YOLO-v11

1. Introduction

The overhead contact system (OCS) is a critical power supply system for high-speed railway operations [1-2]. Insulators play an essential role within the OCS by providing electrical insulation, mechanical support, and potential regulation. If insulator defects occur, then their electrical insulation performance significantly deteriorates, posing severe threats to railway operation safety [3-4]. Therefore, insulator condition monitoring is crucial. The implementation of intelligent defect detection technology can mitigate the risks associated with insulator damage, ensuring the stable operation of the high-speed railway power supply system. Current insulator detection methods predominantly rely on manual data acquisition and analysis. However, when dealing with large volumes of inspection data, manual processing is inherently slow, preventing real-time monitoring and limiting the timely detection and resolution of sudden insulator failures [5-6]. Furthermore, manual detection is susceptible to subjectivity, increasing the likelihood of missed detections and false positives. In addition, due to the high resolution of OCS inspection images, insulator defects occupy only a small portion of the image, further complicating the detection process. Therefore, achieving accurate and efficient intelligent defect detection is essential for identifying potential safety hazards and enhancing the reliability of the railway power supply system.

Deep learning has revolutionized computer vision, expanding its applications across various domains [7-8]. However, in OCS inspection image analysis, existing methods remain largely pattern recognition-based or direct applications of conventional deep learning networks [9-10], lacking in-depth adaptation to real-world scenarios. To address this issue, this study proposed an intelligent insulator defect detection approach based on YOLO-v11 [11], carefully designing the analysis workflow to accommodate the characteristics of OCS inspection images. First, an insulator device positioning model (IDPM) was employed to locate insulators in inspection images. Subsequently, an insulator defect detection model (IDDM) was used for precise defect identification. In addition, a dataset comprising 20,000 OCS inspection images was constructed. Experimental results demonstrated that the proposed method is well-suited for intelligent insulator defect detection, outperforming five state-of-the-art approaches in detection performance. Furthermore, the proposed model exhibited superior generalization capabilities across different insulator types (ceramic insulators and silicone rubber insulators). These findings underscore the substantial application potential of the proposed method in the field of insulator defect detection. This study contributes to the intelligentization of insulator defect detection, enhancing OCS condition monitoring

*E-mail address: huangwei0731@163.com
ISSN: 1791-2377
doi:10.25103/jestr.182.20

efficiency and facilitating the advancement of intelligent high-speed railway maintenance.

2. State of the art

Insulators are exposed to complex and ever-changing natural environments [12-13], and current insulator defect detection predominantly relies on manual data acquisition and analysis, which fails to promptly identify and resolve faults, leading to a high risk of missed detections and false positives [14-15]. Therefore, developing accurate and efficient intelligent defect detection methods is of great significance for ensuring high-speed railway safety. Several studies have explored traditional pattern recognition-based approaches for insulator defect detection. Reference [9] utilized Hu invariant moments and histogram of oriented gradients (HOG) features in combination with support vector machines (SVM) for defect identification. Reference [16] fused pyramid HOG and BOW–SURF features, employing SVM classification for defect detection. Reference [17] detected insulator defects using Harris corner detection and image differencing techniques. These pattern recognition-based methods rely on handcrafted feature design and were limited in their ability to capture diverse defect patterns, restricting their generalization to various defect types. Deep learning, with its superior feature representation capability, enables automatic extraction of critical features from images [18-19], maintaining high performance even in complex scenarios [20-21]. Consequently, researchers have integrated deep learning into insulator defect detection. Reference [22] proposed an insulator defect detection approach based on YOLOv5, incorporating a bidirectional feature pyramid network and squeeze-and-excitation attention mechanism to enhance detection performance. Reference [23] optimized the YOLOv8 network architecture to improve defect detection accuracy. Reference [24] introduced Insu-YOLO, a detection algorithm that fuses multiscale features to enhance insulator defect recognition. Reference [25] further optimized YOLOv8's architecture and training strategies to improve detection precision. Reference [26] developed an insulator defect detection method based on YOLOv5. Reference [27] incorporated Swin Transformer to refine Faster R-CNN, improving defect detection performance in complex backgrounds. Reference [28] introduced high-resolution feature maps, an adaptive spatial feature fusion module, and a deformable attention mechanism to construct a more robust insulator defect detection framework. However, the above methods lack in-depth research adapted to real-world scenarios. The implementation of intelligent detection systems for insulator defects in catenary presents several challenges, as discussed below.

First, existing methods primarily focus on pattern recognition and the application of classical deep learning networks, lacking in-depth research adapted to real-world scenarios.

Second, insulator defect detection methods for catenary that rely on pattern recognition require an analytical model based on prior knowledge, resulting in poor detection performance, insufficient generalization ability, and susceptibility to missed and false detection.

Third, the background of catenary inspection images is complex and susceptible to interference from factors such as illumination and obstacle occlusion. The small size of insulator defects relative to the inspection images significantly increases the detection challenges.

Fourth, the evaluation of detection methods for insulator defects suffers from a scarcity of authentic and representative image datasets. The results did not adequately demonstrate the capability of these methods to suppress false alarms.

To address the above issues, this study proposed a framework specifically designed for insulator defects. Initially, an IDPM was employed to localize insulators within catenary inspection images. Subsequently, an IDDM was used to perform precise defect identification. A catenary inspection image dataset was also constructed to test the performance of the proposed method and compared it with five existing methods. The remainder of this study is structured as follows. Section 3 describes the methodology, Section 4 presents experimental procedures along with result analysis, and the last section concludes this study.

3. Methodology

This study focuses on the construction of an OCS inspection image dataset and the development of an intelligent insulator defect detection method.

As illustrated in Fig.1, the proposed intelligent insulator defect detection method consists of two main stages. First, the IDPM is employed to locate insulators in the inspection images. Next, the IDDM is used to identify insulator defects. If the IDPM fails to detect any insulators, then the image is classified as a non-target image. If an insulator is detected, then the process proceeds to defect identification. If the IDDM detects an insulator defect, then defect information is outputted; otherwise, the image is classified as a non-target image.

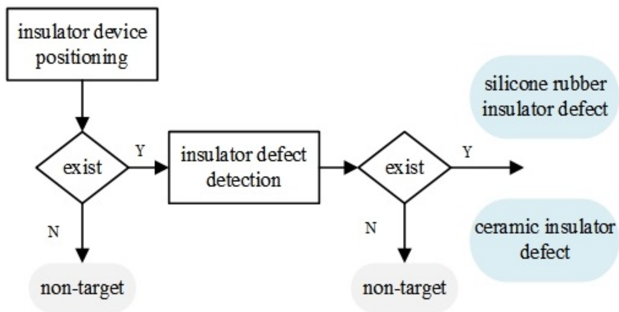

Fig. 1. Intelligent detection method for insulator defects

3.1 OCS inspection image dataset

The OCS inspection image dataset consists of silicone rubber insulators and ceramic insulators, as detailed in Table 1, with representative images shown in Fig.2. This dataset comprises 20,000 images, all with a resolution of 5120×5120 pixels, and each image contains at least one insulator. Particularly, 4,000 images contain defective insulators, whereas 16,000 images contain normal insulators. The inclusion of a large proportion of normal insulators is intended to evaluate the false positive suppression capability of different detection methods, aligning with the actual data distribution in inspection images. Based on the OCS inspection image dataset, an insulator device image dataset was further constructed, which includes 20,000 insulator device images, as shown in Table 2, with representative examples provided in Fig.3.

Table 1. Distribution of imaging conditions in the image dataset

Silicone Rubber Insulator		Ceramic Insulator		Total
number	proportion	number	proportion	number
10000	50.0%	10000	50.0%	20000

Table 2. Distribution of imaging conditions in the image dataset

Type	Normal		Damaged		Total	
	Proportion	Number	Proportion	Number	Proportion	Number
silicone rubber insulator	8000	40.0%	2000	10.0%	10000	50.0%
ceramic insulator	8000	40.0%	2000	10.0%	10000	50.0%
total	16000	80.0%	4000	20.0%	20000	100.0%

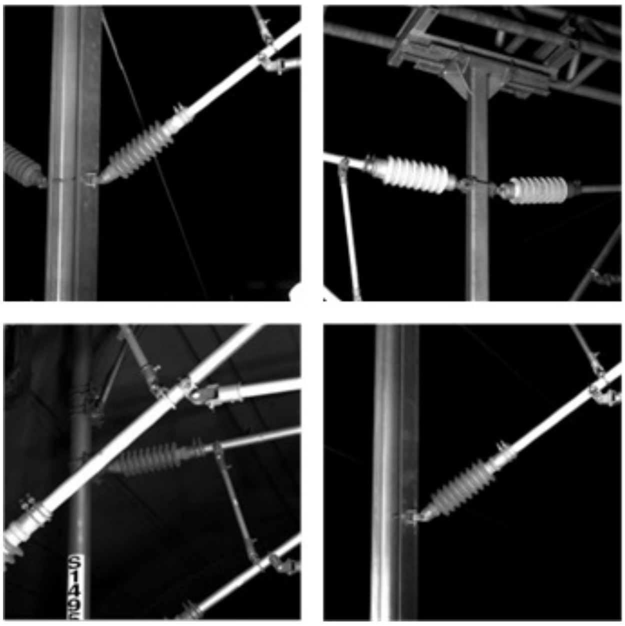

(a) OCS inspection image (including silicone rubber insulators)

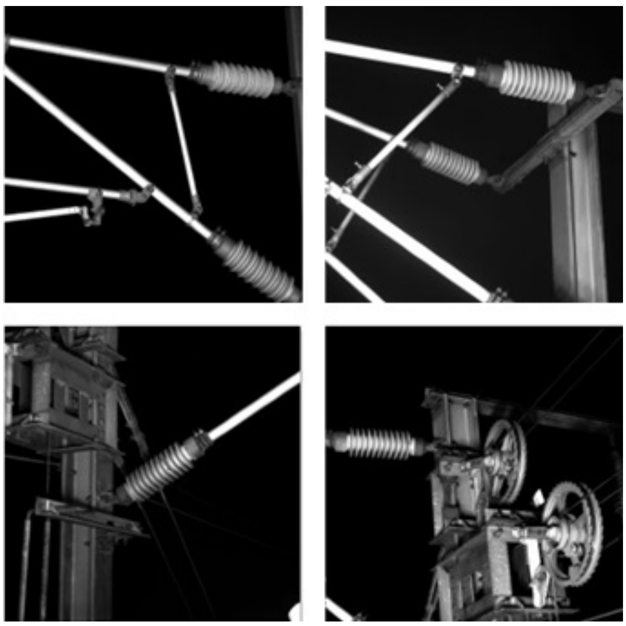

(b) OCS inspection image (including ceramic insulators)

Fig. 2. Typical inspection images of high-speed railway OCS

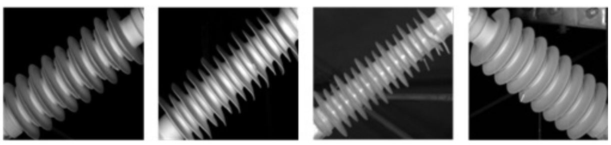

(a) Silicone rubber insulators

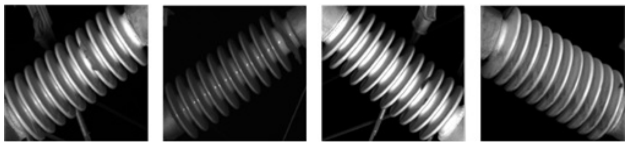

(b) Ceramic insulators

Fig. 3. Typical images of insulator devices

During image annotation, professional OCS inspection personnel manually labeled insulators within the images and classified their insulator types. If an insulator defect was present, then the defect type and location were annotated accordingly.

3.2 Insulator device positioning

Based on an analysis of the characteristics of OCS inspection images, the YOLO-v11 network was selected as the backbone of the IDPM. If no insulators are detected in the inspection image, then the image is classified as a non-target image. If insulators are detected, then the process proceeds to insulator defect identification, as illustrated in Fig.4.

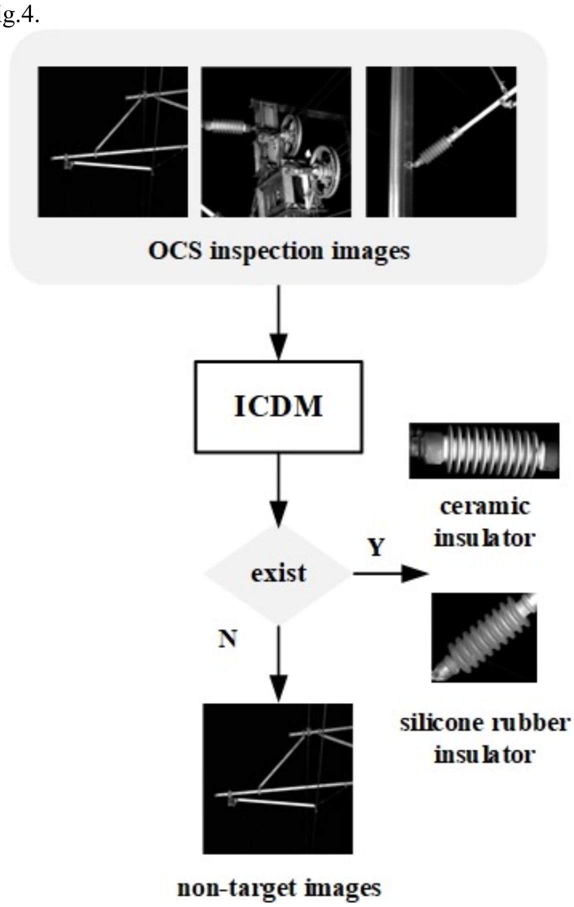

Fig. 4. Positioning process of insulator devices

The process of insulator positioning by the IDPM model within the OCS inspection image dataset $I_{inspect}$ can be expressed as follows:

$$Det_{insul}\left(I_{inspect}\right)=\left\{\left(I_i,D_i\right)\mid I_i\in I_{inspect},D_i\in\{si,ci\}\right\},\tag{1}$$

where I_i represents the *i*-th image in the dataset $I_{inspect}$, and D_i denotes the detected insulator type in the corresponding image I_i (silicone rubber insulator *si* and ceramic insulator *ci*).

3.3 Insulator defect identification

Insulator defects exhibit significant variation in their appearance within images, presenting diverse shapes and sizes, which increases the complexity of identification. For the detected insulator device images, uniform scaling is initially applied, followed by defect identification using the IDDM, as illustrated in Fig.5. The YOLO-v11 network was selected as the backbone for the IDDM. After size normalization, the insulator image was inputted into the IDDM. If no defect is detected, then the image is classified as a non-target image. If a defect is identified, then the system outputs the defect type and location.

Defect identification within the insulator device image dataset I_{insul} can be expressed as follows:

$$\begin{cases} Det_{\text{defect}}\left(I_{insul}\right)=\left(I_j,D_j\right) \\ I_j\in I_{insoul} \\ D_j\in\left\{defect_{si},defect_{ci}\right\} \end{cases},\tag{2}$$

where I_j represents the *j-th* image in the dataset I_{insul}, and D_j denotes the detected defect type I_j in the corresponding image (silicone rubber insulator defect $defect_{si}$ and ceramic insulator defect $defect_{ci}$)

.

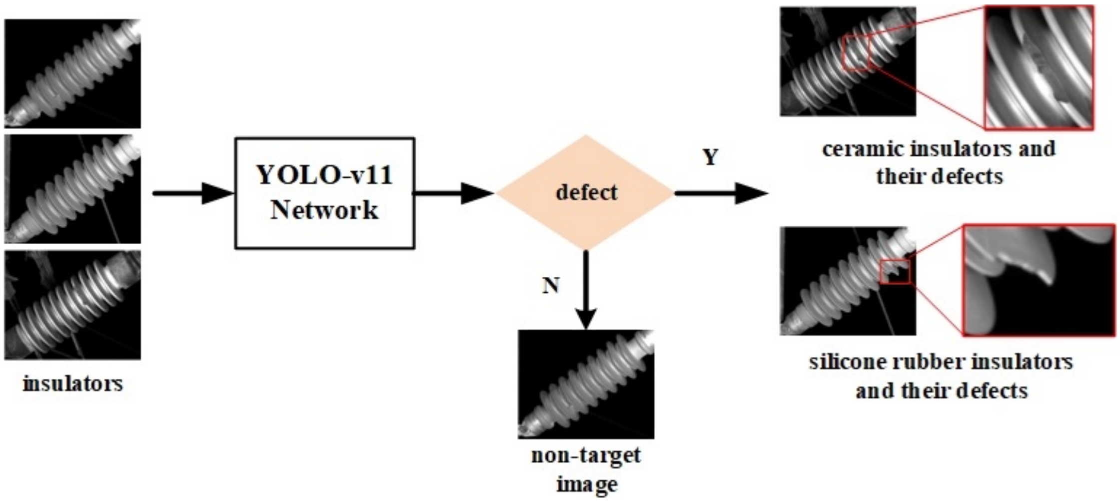

Fig. 5. Recognition of insulator damages

3.4 Key technologies: YOLO-v11 network

The IDPM and IDDM adopt YOLO-v11, whose network architecture is illustrated in Fig.6. The model consists of three main components: backbone, neck, and head. By integrating Transformer, Mosaic data augmentation, and spatial pyramid pooling (SPP) and combining cross-layer feature fusion with a dynamic anchor strategy, the detection performance is significantly enhanced.

(i) Backbone: It is responsible for feature extraction, composed of C3K2 and C2PSA modules. It utilizes the SPP module to fuse multi-scale features.

(ii) Neck: It integrates and enhances features from different layers, generating more robust and discriminative feature representations.

(iii) Head: It predicts detection results, including object class, location, and confidence score.

The loss function of YOLO-v11 is defined in Equation (3), incorporating classification loss L_{cls}, bounding box regression loss L_{box}, and distribution focal loss L_{dfl}. By optimizing classification accuracy, bounding box regression precision, and improving handling of hard samples, the detection performance is significantly enhanced.

$$L=L_{cls}+L_{box}+L_{dfl},\tag{3}$$

The classification loss L_{cls} measures the difference between the predicted class probabilities and ground truth labels. It is based on the cross-entropy loss function, which enhances the prediction accuracy for different object categories.

$$L_{cls}=\sum_{i=0}^{S^2}l_i^{obj}\sum_{c\in classes}\left(p_i(c)-\hat{p}_i(c)\right)^2,\tag{4}$$

where S represents the network grid size, l_i^{obj} indicates whether the *i-th* grid cell contains an object, $p_i(c)$ is the predicted probability that the object in the *i-th* grid cell belongs to category c; and $\hat{p}_i(c)$ is the ground truth label indicating whether the object in the *i-th* grid cell belongs to category *c*.

The bounding box regression loss L_{box} optimizes the difference between the predicted and ground truth bounding boxes. It commonly employs intersection-over-union metrics to measure bounding box overlap, guiding the network's learning process.

$$L_{box} = \lambda_{coord} \sum_{i=0}^{S^2} \sum_{j=0}^{B} l_{ij}^{obj} \left(\left(x_i - \hat{x}_i \right)^2 + \left(x_i - \hat{x}_i \right)^2 \right) + \lambda_{coord} \sum_{i=0}^{S^2} \sum_{j=0}^{B} l_{ij}^{obj} \left(\left(\sqrt{w_i} - \sqrt{\hat{w}_i} \right)^2 + \left(\sqrt{h_i} - \sqrt{\hat{h}_i} \right)^2 \right), \quad (5)$$

where S represents the network grid size; B denotes the number of bounding boxes predicted by each grid cell; l_{ij}^{obj} indicates whether the *j-th* bounding box in the *i-th* grid cell is responsible for predicting the target; x and y correspond to the center coordinates of the bounding box; w and h denote its width and height; and λ_{coord} represents the weight coefficient that balances different loss components

The distribution focal loss L_{dfl} assigns weights to the predicted probabilities of each category, allowing the model to identify and prioritize complex samples.

$$L_{dfl} = -\sum_{i=1}^{N} \sum_{c=1}^{C} y_{ic} * \left(\alpha (1 - p_{ic})^{\gamma} \log(p_{ic}) \right) + y_{ic} * (1 - \alpha) p_{ic}^{\gamma} \log(1 - p_{ic}), \quad (6)$$

where N is the number of samples, C is the number of classes, y_{ic} represents the ground truth label for the *i-th* sample, and p_{ic} is the predicted probability that the *i-th* sample belongs to category c. The balancing factor α adjusts the weight between positive and negative samples, whereas γ controls the weighting of hard samples.

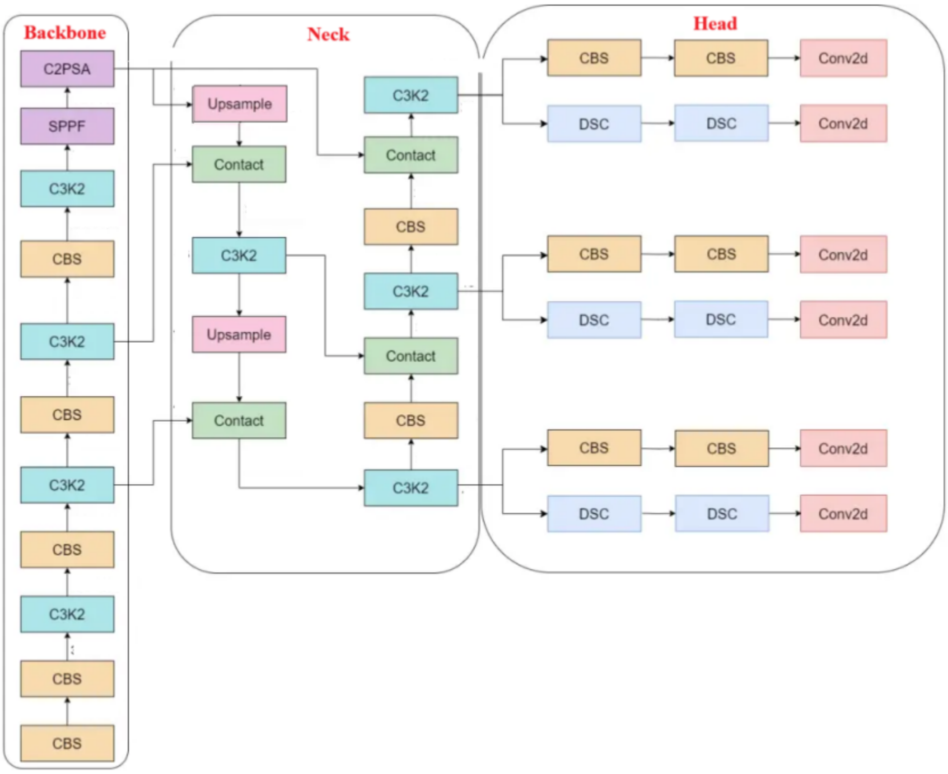

Fig. 6. Network architecture of YOLO-v11

4. Result analysis and discussion

4.1 Experimental setup

At the beginning of training, the IDPM and IDDM load pretrained weights from the COCO dataset, retaining the best-performing weights obtained on the training dataset. The hardware and software configurations are provided in Table 3, and the key parameter settings for YOLO-v11 are listed in Table 4.

Table 3. Hardware Configuration & Software Environment for the Experiment

Hardware and Software	Configuration
CPU	intel core i7
GPU	RTX 3080 12GB (four GPUs)
RAM	128 G
SSD	1TB
Linux	Ubuntu 18.04
Anaconda 3	version 2023.09.0 (64-bit)
CUDA	version 12.1
cuDNN	version 8.2.1

Table 4. Key parameter settings of YOLO-v11 network

Parameter	IDPM	IDDM
nc	2	2
names	["SRI", "CI"]	["SRI_dam", CI_dam"]
optimizer	Adam	Adam
lr0	0.005	0.003
weight_decay	0.0005	0.0003
epochs	120	200
batch size	4	8
patience	10	10
data augmentation	used	used
conf	0.5	0.7

4.2 Performance evaluation metrics

Recall, accuracy, and precision were employed as performance evaluation metrics, as defined in Equations (7)–(9). Higher values indicate better performance. TP denotes true positives, and TN denotes true negatives, representing the number of correctly detected actual targets and correctly rejected non-targets, respectively. FP represents false positives, and FN represents false negatives, denoting the number of misidentified targets and missed targets, respectively.

$$recall = \frac{TP}{TP + FN}, \quad (7)$$

where recall represents the ratio of correctly detected targets to the total number of actual targets.

$$accuracy = \frac{TP + TN}{P + N}, \quad (8)$$

where accuracy denotes the proportion of correctly detected targets out of all evaluated instances.

$$precision = \frac{TP}{TP + FP}, \quad (9)$$

where precision represents the ratio of correctly detected targets to the total number of predicted targets.

4.3 Performance comparison of different networks in insulator localization

Table 5 presents the experimental results for YOLO-v11 and five other detection networks in insulator localization, with results visualized in Fig.7. In Table 5, Row 1 lists the network types used in the comparison, including Faster R-CNN [29], CenterNet [30], EfficientDet [31], YOLO-v5 [32], YOLO-v8 [33], and YOLO-v11. Rows 2 and 3 display the recall and precision achieved by each network on the test set, respectively. Rows 4–5 and 6–7 present the recall and precision obtained on the silicone rubber insulator test subset and ceramic insulator test subset, respectively. Fig.7(a) compares the performance of different networks on the overall test set. Fig.7(b) and 7(c) illustrate the performance comparison on the silicone rubber insulator test subset and ceramic insulator test subset, respectively.

According to Table 5 and Fig.7(a), YOLO-v11 outperforms Faster R-CNN, CenterNet, EfficientDet, YOLO-v5, and YOLO-v8 in terms of recall and precision, demonstrating superior insulator localization performance. As shown in Table 5 and Fig.7(b) and 7(c), for specific insulator types such as silicone rubber insulators and ceramic insulators, YOLO-v11 achieves higher recall and precision compared to the five baseline networks. Faster R-CNN excessively compresses small-object information, leading to missed detections. CenterNet simplifies the network structure, improving detection accuracy, but still has limitations when handling overlapping center points and variations in object size. EfficientDet exhibits good detection performance but is challenging to fine-tune. From YOLO-v5 to YOLO-v8 and YOLO-v11, the continuous introduction of new network structures, optimized anchor box mechanisms, and composite-scale feature fusion has enabled YOLO-v11 to maintain its leading position in object detection. Comparative experiments indicate that YOLO-v11 is well-suited for insulator localization in high-speed railway OCS, achieving robust localization performance in complex railway environments while also demonstrating strong generalization ability across different insulator types.

4.4 Performance comparison of insulator defect detection methods

To verify the effectiveness of the proposed insulator defect detection method, experiments were conducted using the insulator device image dataset, and the results were compared with five representative methods. The experimental results are presented in Table 6, with a bar chart visualization shown in Fig. 8.

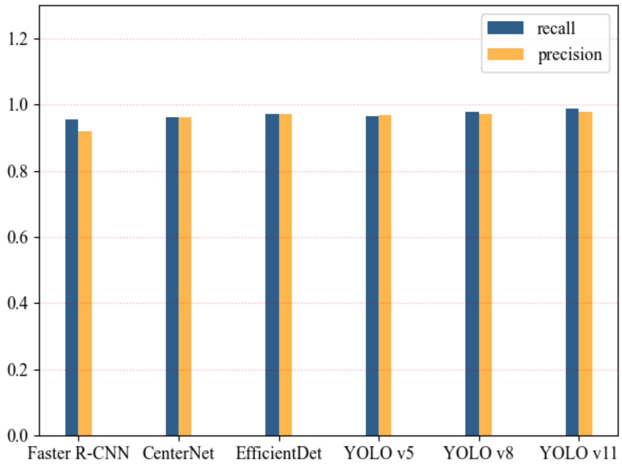

(a) Performance comparison of insulator positioning (silicone rubber insulator and ceramic insulator)

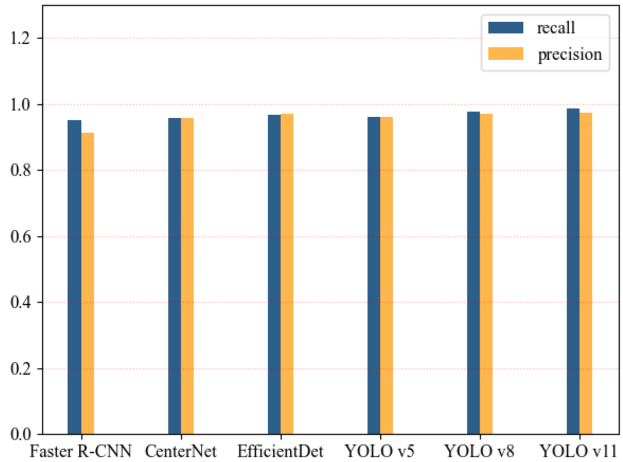

(b) Performance comparison of silicone rubber insulator positioning

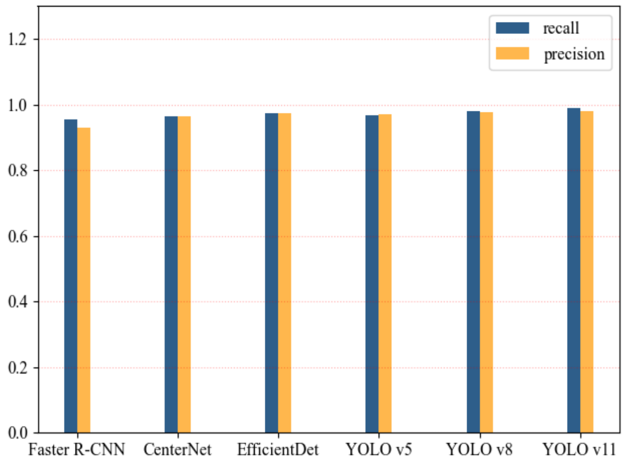

(c) Performance comparison of ceramic insulator positioning

Fig. 7. Performance comparison of insulator positioning by different detection networks

In Table 6, Row 1 lists the method types, where [16], [17], [26], [27], [28], and "proposed" correspond to the methods from references [16], [17], [26], [27], [28], and the proposed method in this study, respectively. Rows 2–4 (recall, accuracy, precision) represent the recall, accuracy, and precision obtained by each method on the test set, respectively. Rows 5–7 and Rows 8-10 (recall (ci), accuracy (ci), and precision (ci)) show the corresponding performance metrics on the silicone rubber insulator test subset and ceramic insulator test subset, respectively.

Table 5. Performance comparison of insulator localization by different networks

	Faster R-CNN	CenterNet	EfficientDet	YOLO-v5	YOLO-v8	YOLO-v11
recall	0.9535	0.9605	0.9703	0.9642	0.9781	**0.9871**
precision	0.9202	0.9609	0.9721	0.9667	0.9729	**0.9769**
recall (si)	0.9518	0.9582	0.9682	0.9626	0.9768	**0.9856**
precision (si)	0.9126	0.9567	0.9698	0.9622	0.9706	**0.9751**
recall (ci)	0.9552	0.9628	0.9724	0.9658	0.9794	**0.9886**
precision (ci)	0.9279	0.9651	0.9745	0.9712	0.9753	**0.9788**

According to Table 6 and Fig.8(a), the proposed method outperforms the five baseline methods in recall, accuracy, and precision, demonstrating superior defect detection performance. Table 6 and Fig.8(b) and 8(c) further indicate that for silicone rubber insulators and ceramic insulators, the proposed method achieves higher recall, accuracy, and precision, exhibiting better generalization capability. Methods [16] and [17] are based on pattern recognition techniques, which have limited feature extraction capabilities, leading to significantly lower recall and precision in defect detection compared to other methods. Methods [26], [27], and [28] leverage deep convectional networks, achieving relatively high defect detection ability (high recall). However, due to limitations in detection methodology and constraints of the specific network architectures used, they suffer from higher false positive rates, resulting in lower accuracy and precision, leaving room for improvement. The proposed method fully considers the imaging characteristics of high-speed railway OCS inspection images and carefully designs the detection process. First, it localizes insulators, addressing the challenge posed by high-resolution inspection images where insulator defects occupy only a small pixel area. Then, it performs precise defect identification on the insulator device images, effectively reducing false positives and improving accuracy and precision. Comparative experiments demonstrate that the proposed method is well-suited for insulator defect detection in high-speed railway OCS, achieving robust performance in complex railway environments while also exhibiting strong generalization ability across different insulator types.

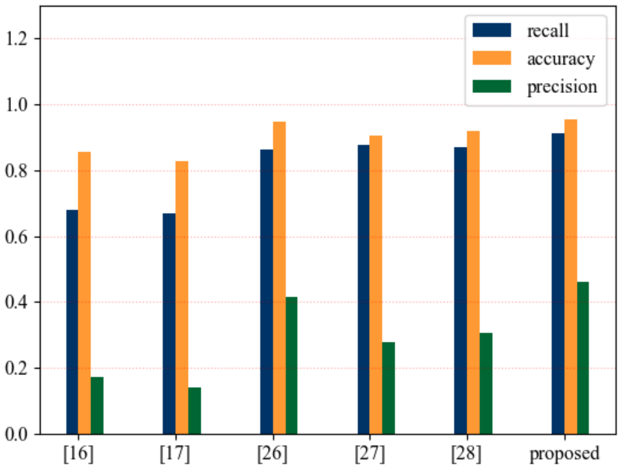

(a) Performance comparison of insulator defect detection methods (silicone rubber insulator and ceramic insulator)

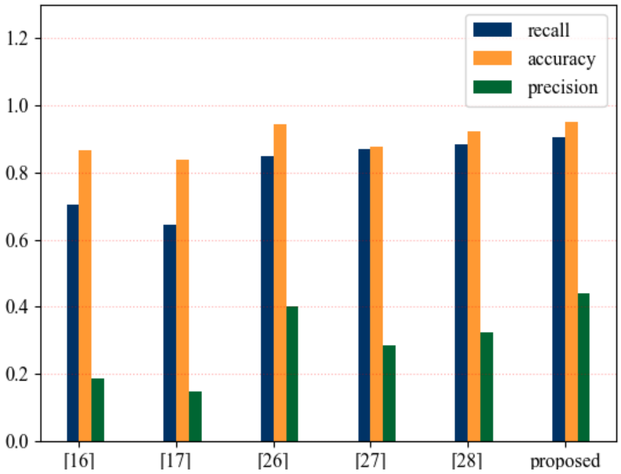

(b) Performance comparison of silicone rubber insulator defect detection methods

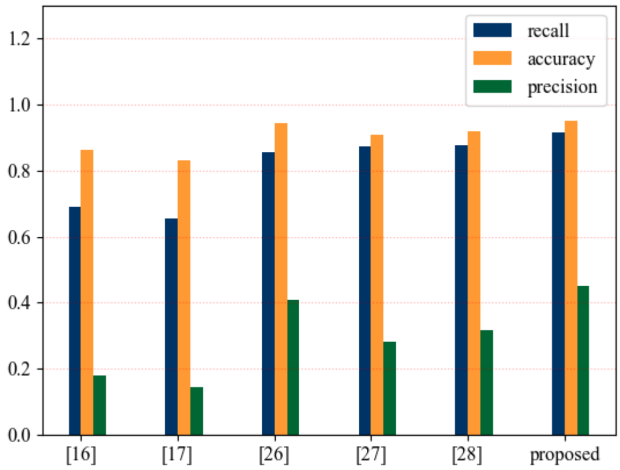

(c) Performance comparison of ceramic insulator defect detection methods

Fig. 8. Performance comparison of insulator defect detection by different methods

4.5 Examples of typical results

This study presents representative examples of the intermediate process and final results of insulator defect detection. Fig.9 and 10 illustrate insulator localization in inspection images, highlighting the algorithm's accuracy and robustness in complex backgrounds. Fig.11 and 12 demonstrate insulator defect detection, showcasing the algorithm's precise defect identification capability. This study also provides the confidence scores of the results, enabling inspection engineers to intuitively assess the reliability of the detection outputs. Specifically, it presents the following:

(1) Insulator localization confidence score: the foreground target probability obtained from the IDPM;

(2) Insulator defect detection confidence score: the type probability output from the IDDM.

Table. 6. Performance comparison of insulator defect detection methods

	[16]	[17]	[26]	[27]	[28]	proposed
recall	0.678	0.670	0.863	0.878	0.870	**0.910**
accuracy	0.856	0.826	0.946	0.905	0.917	**0.954**
precision	0.172	0.143	0.415	0.280	0.308	**0.462**
recall (si)	0.705	0.643	0.848	0.870	0.883	**0.905**
accuracy (si)	0.866	0.837	0.944	0.878	0.922	**0.950**
precision (si)	0.188	0.147	0.403	0.284	0.325	**0.441**
recall (ci)	0.691	0.656	0.855	0.874	0.876	**0.915**
accuracy (ci)	0.861	0.831	0.945	0.907	0.919	**0.952**
precision (ci)	0.179	0.145	0.409	0.282	0.316	**0.451**

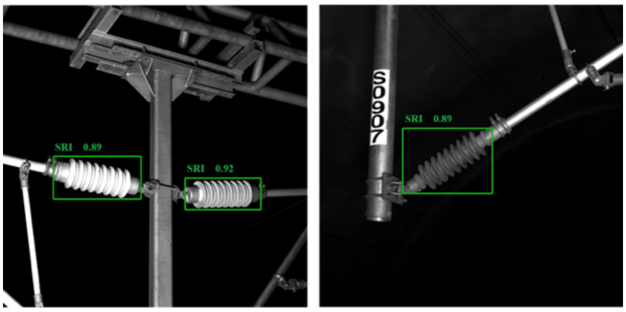

Fig. 9. Positioning of silicone rubber insulators in inspection images

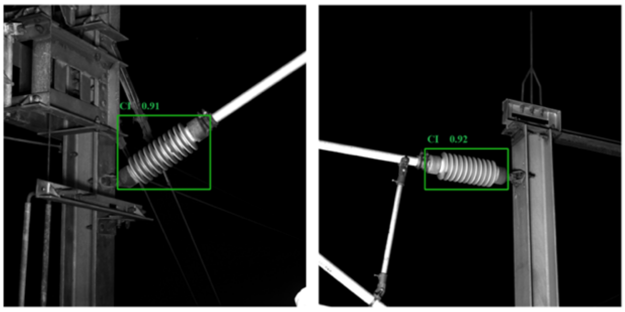

Fig. 10. Positioning of ceramic insulators in inspection images

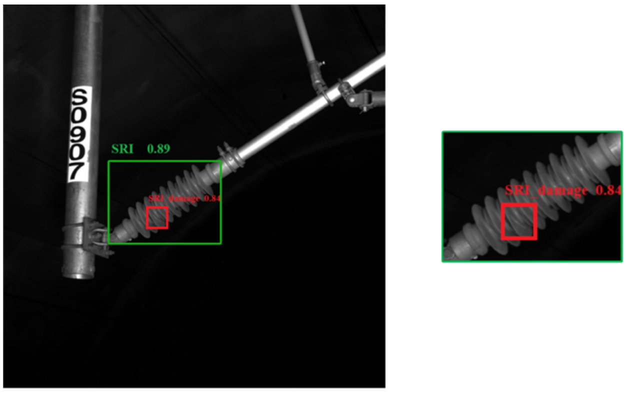

Fig. 11. Defect detection of silicone rubber insulators.

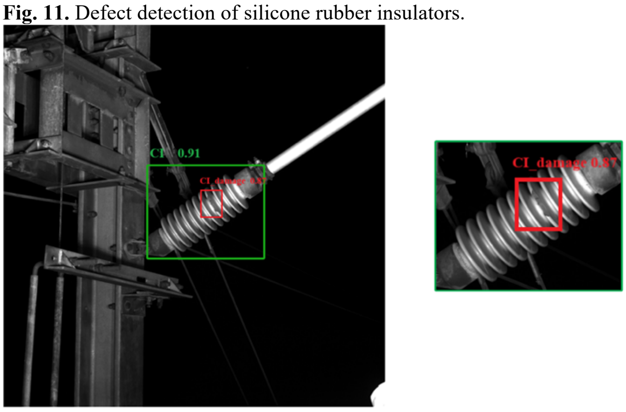

Fig. 12. Detection detection of ceramic insulators

5. Conclusions

For insulator defect detection in high-speed railway OCS, this study proposed an intelligent detection method that follows a device localization–defect identification strategy. First, the IDPM was used to localize insulators from inspection images, followed by the IDDM to accurately identify defects. In addition, a high-speed railway inspection image dataset was constructed. Through insulator localization experiments, defect detection experiments, and result analysis, the following conclusions are drawn:

(1) For insulator defect detection, deep learning models, utilizing multi-layer neural networks, can automatically extract effective features from inspection images, achieving significantly superior performance and generalization compared to pattern recognition methods. Specifically, recall has improved by 0.232–0.240, accuracy by 0.098–0.128, and precision by 0.290–0.319.

(2) The proposed method initially localizes insulators in high-resolution inspection images before identifying defects, effectively addressing the challenge of detecting small defects in high-resolution images using deep neural networks. The proposed method achieves a recall of 0.910, accuracy of 0.954, and precision of 0.462.

(3) The choice of detection network architecture directly determines the performance of insulator localization and defect detection. In addition, the network's overall effectiveness is further influenced by network architecture, loss functions, and training strategies.

(4) The dataset used in experiments must align with the real-world distribution of inspection images to effectively evaluate the model's ability to suppress false positives. Moreover, the dataset should include silicone rubber insulators and ceramic insulators to validate the model's generalization capability.

The proposed method enables accurate detection of insulator defects in high-speed railway OCS, achieving higher recall, accuracy, and precision compared to five baseline methods. This study contributes to enhancing railway operational safety and advancing intelligent inspection of OCS. However, this study also has limitations that require further refinement, including the need to collect more inspection images to improve generalization and enable the detection of a wider variety of defect types.

Acknowledgements
This work was supported by the provincial college student innovation and entrepreneurship training program project (No.S202410644063), the scientific research projects for college students of Sichuan University of Arts and Science (No.X2024Z033), the Sichuan University of Arts and Sciences Education Reform Project (No.2023JG057T), the Key Laboratory of Multi-dimensional Data Sensing and Intelligent Information Processing (No.DWSJ2402), the Key Laboratory of Indoor Space Layout Optimization and Safety

Assurance (No.SNKJ202406 & No.SNKJ202409), the entrusted scientific research projects by enterprises (No.2024HX031 & No.2024HX032), and the Science and Technology Research Project of Jiangxi Provincial Department of Education (No.GJJ2402304), the Natural Science Foundation Project of JiangXi Province (No. 20242BAB25091), and the research projects of Sichuan University of Arts and Science (No.ES202412).

References

[1] M. Mukherjee, R. G. Olsen, and Z. Li. "Non-contact monitoring of overhead transmission lines using space potential phasor measurements," *IEEE Trans. Instrum. Meas.*, vol. 69, no. 10, pp. 7494-7504, Oct. 2020.

[2] Y. G. Lv, W. J. Lou, Z. M. Sun, and H. N. Li. "Numerical simulation of aerodynamic characteristics of three bundled iced transmission lines," *J. Zhejiang Univ. (Eng. Sci. Ed.)*, vol. 44, no. 1, pp. 174-179, Feb. 2010.

[3] A. B. Pablo and H. Alexandra. "Structural performance of porcelain insulators in overhead railway power systems: experimental evaluations and findings," *Infrastructures*, vol. 9, no. 8, Aug. 2024, Art. no. 9080138.

[4] Z. J. Zhang, J. W. You, D. H. Wei, X. L. Jiang, and D. D. Zhang. "Investigations on AC pollution flashover performance of insulator string under different non-uniform pollution conditions," *IET Gener. Transm. Distrib.*, vol. 10, no. 2, pp. 437-443, Feb. 2016.

[5] D. Zhang, S. Gao, L. Yu, G. Kang, X. Wei and D. Zhan. "DefGAN: Defect detection GANs with latent space pitting for high-speed railway insulator," *IEEE Trans. Instrum. Meas.*, vol. 70, Nov. 2020, Art. no. 5003810.

[6] J. Y. Wang, Y. N. Li, and W. X. Chen. "Detection of glass insulators using deep neural networks based on optical imaging," *Remote Sens.*, vol. 14, no. 20, Oct. 2022, Art. no. 5153.

[7] Z. Li, F. Liu, W. Yang, S. Peng, and J. Zhou. "A survey of convolutional neural networks: Analysis, applications, and prospects," *IEEE Trans. Neural Netw. Learn. Syst.*, vol. 33, no. 12, pp. 6999-7019, Dec. 2022.

[8] Y. Zhang, C. Zhang, and Y. H. Z. Tang. "Cross-modal concept learning and inference for vision-language models," *Neurocomputing*, vol. 583, no. 28, May 2024, Art. no. 127530.

[9] J. Shi, J. Zhang, and H. H. Zhong. "Catenary insulator fault detection based on gradient image fusion," *Infrared Tech.*, vol. 45, no. 10, pp. 1106-1117, Oct. 2023.

[10] Y. X. Liu, X. D. Li, R. Y. Qiao, Y. Chen, X. L. Han and A. Paul. "Lightweight insulator and defect detection method based on improved YOLOv8," *Appl. Sci.*, vol. 14, , no. 19, Sep. 2024, Art. no. 8691.

[11] J. Glenn and Q. Jing. "yolo_v11_grazpedwri dataset." github.com. Accessed: Sep. 12, 2024. [Online.] Available: https://universe.roboflow.com/tesisdiazfinal/yolo_v11_grazpedwri.

[12] X. H. Qiao, Z. J. Zhang, X. L. Jiang, S. D. Raji, X. D. Ma and X. Li. "AC failure voltage of iced and contaminated composite insulators in different natural environments," *Int. J. Electr. Power Energy Syst.*, vol. 120, , no. 5, Mar. 2020, Art. no. 105993.

[13] U. Pramuk and P. Siamrat. "Influence of relative humidity on surface charge decay on epoxy resin insulators," *Energy Procedia*, vol. 89, pp. 110-119, June. 2016.

[14] Y. Guo, M. L. Ma, and D. L. Li. "Detection of surface defects in lightweight insulators using improved YOLOv5," *Laser Optoelectron. Prog.*, vol. 60, no. 24, Dec. 2023, Art. no. 2412007.

[15] J. P. Zhong, Z. G. Liu, C. Yang, H. R. Wang, S. B. Gao and A. Núñez. "Adversarial reconstruction based on tighter oriented localization for catenary insulator defect detection in high-speed railways," *IEEE Trans. Intell. Transp. Syst.*, vol. 23, no. 2, pp. 1109-1120, Feb. 2022.

[16] G. C. Chen, G. M. Gu, X. N. Yu, and Z. B. Li. "Method for defect detection of catenary insulators by combining the features of phog and bow-surf," *J. Chin. Mini-Micro Comput. Syst.*, vol. 42, no. 1, pp. 172-177, Jan. 2021.

[17] X. X. Guo., Z. G. Liu, G. N. Zhang, and S. B. Gao. "Fault detection of catenary insulator based on corner matching and image differencing," *Artif. Intell. Rev.*, vol. 27, no. 2, pp. 8-14, Feb. 2024.

[18] Y. X. Ma, J. X. Yin, F. Huang, and Q. P. Li. "Surface defect inspection of industrial products with object detection deep networks: A systematic review," *Artif. Intell. Rev.*, vol. 57, no. 12, Oct., 2024, Art. no. 333.

[19] Z. Y. Song, L. Liu, F. Y. Jia, Y. D. Luo, C. Y. Jia and G. X. Zhang. "Robustness-aware 3D object detection in autonomous driving: A review and outlook," *IEEE Trans. Intell. Transp. Syst.*, vol. 25, no. 11, pp. 15407-15436, Nov. 2024.

[20] Z. Q. Zhao, P. Zheng, S. T. Xu, and X. Wu. "Object detection with deep learning: A review," *IEEE Trans. Neural Netw. Learn. Syst.*, vol. 30, no. 11, pp. 3212-3232, Nov. 2019.

[21] B. Ganga, B. T. Lata, and K. R. Venugopal. "Object detection and crowd analysis using deep learning techniques: Comprehensive review and future directions," *Neurocomputing*, vol. 597, no. 7, pp. 1-32, Sep. 2024.

[22] Y. L. Zhang, Y. M. Zhang, L. Mu, X. H. Xue, J. Huang and X. S. Xie, "A novel convolutional neural network-based insulator defect detection method for high-voltage transmission lines," in Proc. Int. Conf. Intel. UAV. Sys.. Springer, Singapore, Singapore, 2024, pp. 223-231.

[23] G. G. Tan, Y. S. Ye, J. W. Chu, Q. Liu, L. Xu and B. Wen. "Real-time detection method of intelligent classification and defect of transmission line insulator based on lightweight-YOLOv8n network," *J. Real-Time Image Proc.*, vol. 22, Jan. 2025, Art. no. 53.

[24] Y. Chen, H. Liu, J. Chen, J. Hu, and E. Zheng. "Insu-YOLO: An insulator defect detection algorithm based on multiscale feature fusion," *Electronics*, vol. 12, no. 15, pp. 192-207, Jul. 2023.

[25] L. Zhang, B. Li, and L. J. Gao. "Research on improved YOLOv8 algorithm for insulator defect detection," *J. Real-Time Image Proc.*, vol. 21, no. 1, Jan. 2024, Art. no. 22.

[26] N. Zhang, J. Su, Y. Zhao, and H. Chen. "Insulator-YOLO: Transmission line insulator risk identification based on improved YOLOv," *Processes*, vol. 12, no. 11, Nov. 2024, Art. no. 2552.

[27] Y. Xi, K. Zhou, and L. W. Meng. "Transmission line insulator defect detection based on swin transformer and context," *Mach. Intell. Res.*, vol. 20, no. 5, pp. 729-740, Sep. 2023.

[28] X. Lu, C. L. Jiang, Z. J. Ma, H. T. Li, and Y. X. Liu. "A simple and effective surface defect detection method of power line insulators for difficult small objects," *Comput. Mater. Contin.*, vol. 79, no. 1, pp. 373-390, Apr. 2024.

[29] S. Q. Ren, K. M. He, R. Girshick, and J. Sun. "Faster R-CNN: Towards real-time object detection with region proposal networks," *IEEE Trans. Pattern Anal. Mach. Intell.*, vol. 39, no. 6, pp. 1137-1149, Jun. 2017.

[30] K. W. Duan, S. Bai, H. Qi, Q. N. Huang and Q. Tian, "CenterNet: Keypoint triplets for object detection," in Proc. IEEE/CVF Int. Conf. Comput. Vis. (*ICCV 2019*), Seoul, Korea, 2019, pp. 6568-6577.

[31] M. Tan, R. Pang, and Q. V. Le, "EfficientDet: Scalable and efficient object detection," in Proc. IEEE Conf. Comput. Vis. Pattern Recog. (CVPR 2020), Seattle, WA, USA, 2020, pp. 10778-10787.

[32] G. Jocher. "Yolov5." github.com. Accessed: Feb. 1, 2020. [Online.] Available: https://github.com/ultralytics/yolov5.

[33] G. Jocher, A. Chaurasia, and J. Qiu. "Ultralytics YOLO (Version 8.0.0)." github.com. Accessed: Jan. 4, 2023. [Online.] Available: https://github.com/ultralytics/ultralytics.